The Astrophysical Journal, 952:105 (10pp), 2023 August 1 https://doi.org/10.3847/1538-4357/acd755

Looking for Traces of Nonminimally Coupled Dark Matter in the X-COP Galaxy Clusters Sample

Giovanni Gandolfi[1,2,3], Balakrishna S. Haridasu[1,2,3], Stefano Liberati[1,2,3], and Andrea Lapi[1,2,3,4]
[1] SISSA, Via Bonomea 265, I-34136 Trieste, Italy; giovigandolfi@gmail.com
[2] IFPU—Institute for Fundamental Physics of the Universe, Via Beirut 2, I-34014 Trieste, Italy
[3] INFN-Sezione di Trieste, via Valerio 2, I-34127 Trieste, Italy
[4] IRA-INAF, Via Gobetti 101, I-40129 Bologna, Italy
Received 2022 November 15; revised 2023 May 17; accepted 2023 May 18; published 2023 July 20

Abstract

We look for possible evidence of a nonminimal coupling (NMC) between dark matter (DM) and gravity using data from the X-COP compilation of galaxy clusters. We consider a theoretically motivated NMC that may dynamically arise from the collective behavior of the coarse-grained DM field (e.g., via Bose–Einstein condensation) with averaging/coherence length $L_{\rm NMC}$. In the Newtonian limit, the NMC modifies the Poisson equation by a term $L_{\rm NMC}^2\nabla^2\rho$ proportional to the Laplacian of the DM density itself. We show that this term, when acting as a perturbation over the standard Navarro–Frenk–White (NFW) profile of cold DM particles, can yield DM halo density profiles capable of correctly fitting galaxy clusters' pressure profiles with an accuracy comparable to and, in some cases, even better than the standard cold DM NFW profile. We also show that the observed relation between the NMC length scale and the virial mass found in Gandolfi et al. for late-type galaxies is consistent with the relation we find in the current work, suggesting that the previously determined power-law scaling law holds up to galaxy cluster mass scales.

Unified Astronomy Thesaurus concepts: Cold dark matter (265); Galaxy clusters (584); Dark matter (353); Non-standard theories of gravity (1118); Cosmology (343)

1. Introduction

Zwicky (1933) originally hypothesized the existence of an unseen matter component to explain the large velocity scatter of the Coma cluster. In subsequent decades, astrophysicists became aware of a discrepancy between luminous matter and the amount of mass required to explain the kinematic properties of spiral galaxies (Bosma 1978; Rubin et al. 1978). The astrophysical community traces back this missing mass to dark matter (DM); an unseen, cold (i.e., nonrelativistic), and weakly interacting massive particle. This cold DM paradigm has been successful on cosmological scales, yet it struggles to fully reproduce the observed phenomenology on galactic scales, especially in DM-dominated dwarfs. This has motivated astrophysicists to consider several possible solutions, some of them radically departing from the standard cold DM paradigm. Some astrophysicists advocate a more realistic and complete inclusion of baryonic physics and feedback in models and simulations that could in principle alleviate some of the cold DM phenomenological issues at galactic scales (see, e.g., Di Cintio et al. 2014; Pontzen & Governato 2014; El-Zant et al. 2016; Santos-Santos et al. 2016; Desmond 2017; Keller & Wadsley 2017; Ludlow et al. 2017; Navarro et al. 2017; Peirani et al. 2017; Wheeler et al. 2019; Freundlich et al. 2020a, 2020b). Others point to alternative scenarios in which DM is composed of nonstandard particle candidates (see the review by Salucci 2019 and references therein). Another proposal was to abandon entirely the DM paradigm in favor of modifying the laws of gravity (such as in the modified Newtonian dynamics or MOND model, originally proposed in Milgrom 1983).

In Gandolfi et al. (2021) and Gandolfi et al. (2022), we have explored a new possibility to solve the small-scale incompleteness of the cold DM paradigm, having reviewed and tested a model in which cold DM is nonminimally coupled with gravity. Many other works by our team and collaborators already conjectured this possibility (e.g., Bruneton et al. 2009; Bertolami 2010; Bettoni et al. 2011, 2014; Bettoni & Liberati 2015; Ivanov & Liberati 2020). As shown in Gandolfi et al. (2021) and Gandolfi et al. (2022), the introduction of this coupling extends in a simple fashion the cold DM paradigm while maintaining its successful phenomenology on large cosmological scales and improving its behavior in galactic systems. The term "nonminimal" implies that the gradient of the DM distribution directly couples with the Einstein tensor. Such nonminimal coupling (NMC) is not necessarily a fundamental feature of the DM particles but rather may dynamically develop when the averaging/coherence length $L_{\rm NMC}$ associated with the fluid description of the DM collective behavior is comparable to the local curvature scale. In the Newtonian limit, this NMC appears as a modification of the Poisson equation by a term $L_{\rm NMC}^2\nabla^2\rho$ proportional to the DM density ρ (see Bettoni et al. 2014). This simple modification impacts the internal dynamics of spiral galaxies, which are altered compared to a pure cold DM framework. In Gandolfi et al. (2021) and Gandolfi et al. (2022) we have shown that this NMC between DM and gravity can alleviate the so-called core–cusp controversy, i.e., the observed discrepancy between the cored inner radii shape of the observed galactic dark haloes' density profiles with the cuspier shape predicted by DM, gravity-only simulations that are best described by the so-called Navarro–Frenk–White (NFW) profile (Navarro et al. 1996; Łokas & Mamon 2001;

Boylan-Kolchin & Ma 2004; Navarro 2006; de Blok 2010; Navarro et al. 2017). Gandolfi et al. (2022) have also shown how such NMC manages to reproduce for a diverse sample of spiral galaxies the tight empirical relationships linking the baryonic and the dark component of galaxies. It is argued that the most general of such relations is the radial acceleration relation (see Lelli et al. 2017; Chae et al. 2019; Li et al. 2018; Di Paolo et al. 2019; Green & Moffat 2019; Rodrigues & Marra 2020; Tian et al. 2020), whose explanation is far from trivial in the cold DM framework (albeit some attempts have been made in this sense; see, e.g., Di Cintio et al. 2014; Di Cintio & Lelli 2016; Santos-Santos et al. 2016; Desmond 2017; Keller & Wadsley 2017; Ludlow et al. 2017; Navarro et al. 2017; Wheeler et al. 2019).

The aim of the present work is to test the NMC DM model on the scales of galaxy clusters to assess its capability in fitting their pressure profiles and to determine if the scale relations predicted by this model are also satisfied in these regimes. For this purpose we will use the XMM-Newton Cluster Outskirts Project (X-COP) data products (see Ghirardini et al. 2018, 2019; Eckert et al. 2019; Ettori et al. 2019). This sample consists of 12 clusters with well-observed X-ray emission and high signal-to-noise ratio in the Planck Sunyaev–Zel'dovich (SZ) survey (Planck Collaboration et al. 2016). With the X-COP data we would have information about the intracluster medium (ICM) temperature and pressure in a wide radial range, from 0.2 to 2 Mpc.

The paper is organized as follows: in Section 2 we will briefly summarize the underlying theory behind the NMC DM model, and we will present the data of the X-COP collaboration in more detail; in Section 3 we will proceed to illustrate and comment on our results, and in Section 4 we will summarize our work as well as outline the future developments of our work.

Throughout this work, we adopt the standard flat ΛCDM cosmology (Aghanim et al. 2020) with rounded parameter values: matter density $\Omega_M = 0.3$, dark energy density $\Omega_\Lambda = 0.7$, baryon density $\Omega_b = 0.05$, and Hubble constant $H_0 = 100h\,\mathrm{km\,s^{-1}\,Mpc^{-1}}$ with $h = 0.7$. Unless otherwise specified, $G \approx 6.67 \times 10^{-8}\,\mathrm{cm^3\,g^{-1}\,s^{-2}}$ indicates the standard gravitational (Newton) constant.

2. NMC Modeling and X-COP Data

2.1. A Theoretical Background for the NMC

Here we provide a short theoretical background for the NMC DM model, referring the reader to Gandolfi et al. (2021) and Gandolfi et al. (2022) for further information. A very basic NMC model can be built with the addition of a coupling term $S_{\rm int}$ between DM and gravity in the total Einstein–Hilbert action (in the Jordan frame) with shape:

$$S_{\rm int}\,[\tilde{g}_{\mu\nu},\,\varphi] = \epsilon L_{\rm NMC}^2 \int \mathrm{d}^4x\,\sqrt{-\tilde{g}}\;\widetilde{G}^{\mu\nu}\,\nabla_\mu\varphi\nabla_\nu\varphi\;; \qquad (1)$$

here φ is the (real) DM scalar field, $\epsilon = \pm 1$ is the polarity of the coupling, $\widetilde{G}^{\mu\nu}$ is the Einstein tensor, and $L_{\rm NMC}$ is the NMC characteristic length scale. From a purely theoretical perspective, such a form of the NMC is allowed by the Einstein equivalence principle (e.g., Bekenstein 1993; Di Casola et al. 2015). In our approach, however, the length $L_{\rm NMC}$ does not need to be a new fundamental constant of nature as it is indeed suggested by its virial mass-dependent scaling observed in Gandolfi et al. (2022). Instead, $L_{\rm NMC}$ could emerge dynamically from some collective behavior of the coarse-grained DM field (e.g., Bose–Einstein condensation). We hence remark that our NMC model does not consist in a modified gravity theory but simply in a formalization of an emergent behavior of cold DM inside halos. Furthermore, the bookkeeping parameter ϵ will be set to $\epsilon = -1$ (repulsive coupling) based on the findings of Gandolfi et al. (2021) and Gandolfi et al. (2022).

We also stress that the NMC DM model hereby discussed could in principle share features with other prospective DM models, such as self-interacting DM scenarios. Nonetheless, the NMC DM framework contemplates not only a self-interaction term for DM in the action but also a scale-dependent geometric interaction term between the DM field and the baryonic component, which is sourced by the NMC of the DM to gravity.

Adopting the fluid approximation for the field φ (as in Bettoni et al. 2012) and taking the Newtonian limit, the NMC translates into a simple modification of the Poisson equation (Bettoni et al. 2014)

$$\nabla^2\Phi = 4\pi G[(\rho + \rho_{\rm bar}) - \epsilon L^2\nabla^2\rho], \qquad (2)$$

where Φ is the Newtonian potential, and $\rho_{\rm bar}$ and ρ are the baryonic and DM densities. In spherical symmetry, Equation (2) implies that the total gravitational acceleration writes

$$g_{\rm tot}(r) = -\frac{G\,M(<r)}{r^2} + 4\pi\,G\,\epsilon L^2\,\frac{\mathrm{d}\rho}{\mathrm{d}r}, \qquad (3)$$

where $M(<r)$ is the total mass enclosed in the radius r; the first term is the usual Newtonian acceleration, and the second term is the additional contribution from the NMC.

In Gandolfi et al. (2021) we have highlighted that Equation (2) gives rise to some interesting features for strongly DM-dominated systems in self-gravitating equilibria. First of all, the NMC can help to develop an inner core in the DM density profile. This enforces a shape for the density profile, which closely follows the phenomenological Burkert profile (Burkert 1995) out to several core scale radii. Moreover, DM-dominated halos with NMC are consistent with the core-column density relation (see, e.g., Salucci & Burkert 2000; Donato et al. 2009; Behroozi et al. 2013; Burkert 2015, 2020), i.e., with the observed universality of the product between the core radius r_0 and the core density ρ_0. In Gandolfi et al. (2022) we tested the NMC hypothesis using a diverse sample of spiral galaxies. The NMC DM model proved to yield fits to the stacked rotation curves of such objects with a precision always superior to pure NFW model fits and in several instances comparable to or even better than the Burkert model ones. Furthermore, we observed an interesting power-law scaling relation between the halo virial mass M_{200} and the NMC length scale $L_{\rm NMC}$ for the fitted galaxies. By assuming such mass-dependent scaling of $L_{\rm NMC}$, the NMC DM model was also able to reproduce the radial acceleration relation up to the regime of dwarf spheroidal galaxies. Yet the NMC DM model awaits testing on scales larger than galactic ones, and this is precisely the scope of the present work.

Table 1
Reduced χ^2 and Bayesian Evidence $\Delta_{\mathcal{B}}$ from the MCMC Analysis for the NFW and NMC DM Models

Cluster	z	$\chi^2_{\rm red,NFW}$	$\chi^2_{\rm red,NMC}$	$\Delta_{\mathcal{B}}$
A85	0.0555	2.9	2.7	−0.89
A644	0.0704	2.4	2.2	0.11
A1644	0.0473	3.9	3.4	1.01
A1759	0.0622	1.7	1.6	1.34
A2029	0.0773	1.6	1.6	−0.15
A2142	0.0909	3.3	3.3	−1.32
A2255	0.0809	6.7	1.8	2.64
A2319	0.0557	7.8	7.1	2.05
A3158	0.0597	2.3	2.1	2.81
A3266	0.0589	6.7	6.8	−1.89
RXC1825	0.0650	3.3	6.1	−3.53
ZW1215	0.0766	0.97	0.86	−0.81

Note. The Bayesian evidence $\Delta_{\mathcal{B}}$ is calculated in favor of the NMC DM model.

2.2. Modeling Cluster Thermal Profiles

The thermal pressure profiles[5] of galaxy clusters are defined as functions of the gravitational potential in play. In the framework of the NMC DM model this reads as

$$P^{\rm th}(R) = P^{\rm th}(0) - 1.8\mu m_{\rm p}\int_0^R n_{\rm e}(r)\left[\frac{GM_{\rm DM}(r)}{r^2} - 4\pi\, G\, \epsilon L^2_{\rm NMC}\,\frac{{\rm d}\rho}{{\rm d}r}\right]{\rm d}r, \tag{4}$$

where we model the electron density (ED) profile through the Vikhlinin profile (Vikhlinin et al. 2006),

$$\frac{n_e(r)}{n_0} = \frac{(r/r_c)^{-\alpha/2}[1+(r/r_s)^{\gamma}]^{-\varepsilon/(2\gamma)}}{[1+(r/r_c)^2]^{(3/2)\beta-\alpha/4}}. \tag{5}$$

To specify the dark mass distribution in Equation (4) we adopt the same perturbative approach of Gandolfi et al. (2022), considering the NMC as a small perturbation over the standard cold DM NFW profile

$$\rho_{\rm NFW}(r) = \frac{\delta_{\rm c}\rho_{\rm c} r_s^3}{r(r+r_s)^2}. \tag{6}$$

Here, r_s is the reference scale radius, δ_c is the dimensionless characteristic overdensity of the halo, and $\rho_{\rm c} = 3H_0^2/8\pi G$ is the local critical density. The NFW profile can also be written in terms of the halo virial mass M_{500} (i.e., the mass value at which the interior mean density is 500 times the critical density of the universe), and the halo concentration $c \equiv r_{500}/r_s$, with $r_{500} \approx 260(M_{500}/10^{12}M_{\odot})^{1/3}$ being the virial radius, and $\delta_c\rho_c = M_{500}c^3 g(c)/4\pi r_{500}^3$ with $g(c) \equiv [\ln(1+c) - c/(1+c)]^{-1}$. The DM mass profile in Equation (4) will then coincide with the NFW mass distribution, and the term $d\rho/dr$ will be the gradient of the NFW density profile. We remark that in this analysis the perturbative parameter is $L_{\rm NMC}/r_s$, a quantity that is always small for the range of masses probed in our study, as we will show with our results.

[5] Here the gas density $n_{\rm gas}(r) \approx 1.826\, n_e(r)$ is the sum of the electron and proton number densities, μ is the mean molecular weight in atomic mass units, and m_p is the proton mass.

2.3. The X-COP Data

We test the aforementioned formalism for the NMC using the X-COP[6] catalog (Eckert et al. 2017) with joint X-ray temperature and SZ pressure observations. The methodology we adopt here is equivalent to the one earlier implemented in Haridasu et al. (2021; please refer to it for further details). To constrain the characteristic length scale ($L_{\rm NMC}$) alongside the parameters of the mass profile (Θ_M) and the ED (Θ_e), we write a joint likelihood $\mathcal{L}$ as

$$\mathcal{L} = \mathcal{L}_{\rm P_X} + \mathcal{L}_{\rm P_{SZ}} + \mathcal{L}_{\rm ED}, \tag{7}$$

where the pressure is computed through Equation (4) and the ED is modeled as Equation (5). Here the first term accounts for the likelihood corresponding to the X-ray temperature $P_{\rm X}$ data, the second term denotes the likelihood for the covarying SZ pressure data, and the last term in Equation (7) accounts for the modeled ED data.

Alongside these primary parameters of the model we also include an additional intrinsic scatter $\Sigma_{\rm P,\ int}$, following the approach in Ghirardini et al. (2018) and Ettori et al. (2019). We refer to Haridasu et al. (2021) for an elaborate discussion on the mild differences between our approach here and the analysis performed in Ettori et al. (2019).

We perform a Bayesian analysis through MCMC sampling using the publicly available `emcee`[7] package (Foreman-Mackey et al. 2013; Hogg & Foreman-Mackey 2018), which implements an affine-invariant ensemble sampler and `GetDist`[8] package (Lewis 2019), to perform analysis of the chains and plot the contours. We utilize flat uniform priors on all the parameters $\Theta_e = \{n_0, \alpha, \beta, \varepsilon, r_{\rm c}, r_{\rm s}\}$, $\Theta_{\rm M} = \{M_{500}, c\}$, and the NMC characteristic length scale $L_{\rm NMC}$ in the MCMC analysis. Note here that we utilize the analytical form for the $M(<r)$ of the cluster, which is expressed as a function of $\Theta_{\rm M}$. Finally, we also perform a model comparison through the Bayesian evidence $\mathcal{B}$ (Trotta 2008, 2017; Heavens et al. 2017b) using the `MCEvidence`package (Heavens et al. 2017a).[9] Comparing the Bayesian evidence, one can assess the preference for a given model $\mathcal{M}_{\rm l}(\Theta_{\rm l})$ over the base model, i.e., the NFW model. Also, the Bayesian evidence is contrasted on the Jeffreys scale (Jeffreys 1961), where $\Delta\log(\mathcal{B}) < 2.5$ and $\Delta\log(\mathcal{B}) > 5$, implying either a weak or a strong preference for the extended model, respectively.

3. Testing the NMC with X-COP Galaxy Clusters Data

3.1. General Results and Example Clusters

We report the results of our MCMC parameter estimation in Table 2 and the respective statistical comparison in Table 1. The reduced chi-squared ($\chi^2_{\rm red}$) values in Table 1 indicate that for the majority of the clusters, the NMC DM model generally provides a description of the data comparable to and often even better than the NFW model. Nevertheless, we point out that the value of the NMC length scale $L_{\rm NMC}$ is partially guided by the availability of data at the innermost radii, and X-COP cluster pressure profiles are not well characterized in these regions. This lack of data at small radii relaxes the constraints on the higher end of the possible values for $L_{\rm NMC}$, and it is ultimately

[6] The datasets are publicly available at the following link: https://dominiqueeckert.wixsite.com/xcop/about-x-cop.
[7] http://dfm.io/emcee/current/
[8] https://getdist.readthedocs.io/
[9] https://github.com/yabebalFantaye/MCEvidence

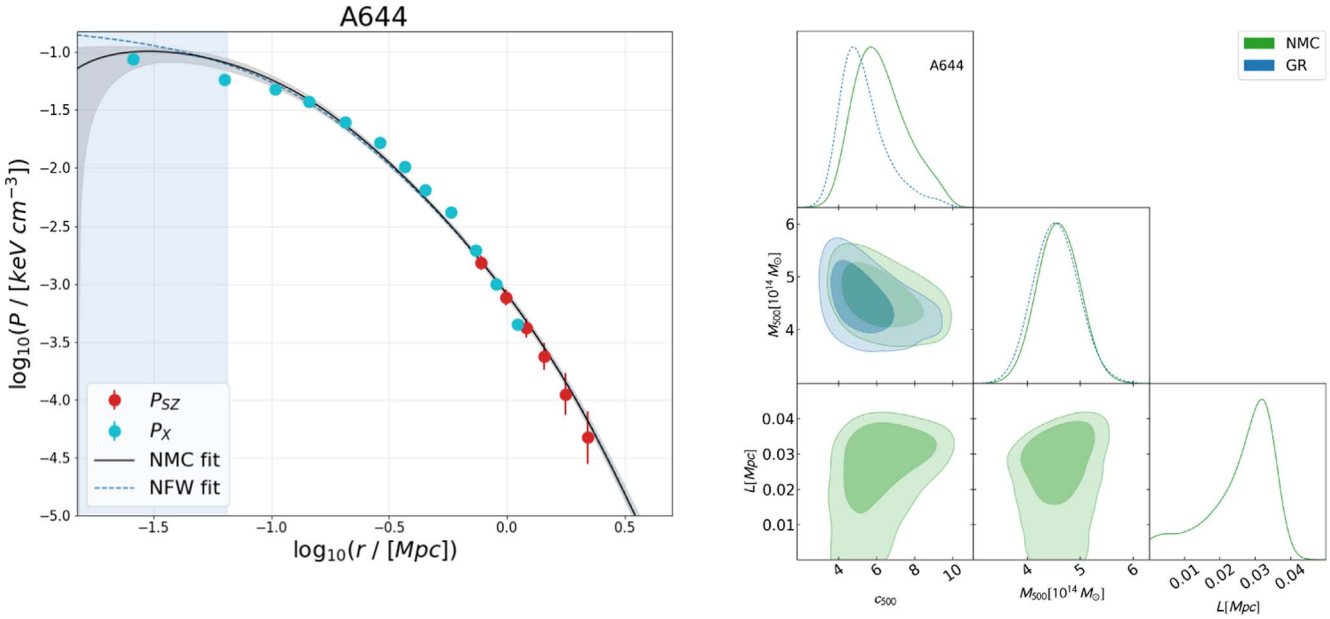

Figure 1. Left: pressure profile and related contour plots for the A644 cluster. Data are displayed as red dots (SZ effect data) and cyan dots (data from the temperature profile by X-ray measurements). The solid black lines represent the Bayesian MCMC best fit for the NMC DM model, with the gray contour representing the 68% confidence interval around the best-fit line. The dashed blue line represents the NFW best fit. The blue shaded area in the profile represents the region of the dark halo within which the NMC is active, i.e., an area that extends from the center of the halo up until $L_{\rm NMC}$. Right: the green contours represent the NMC DM model, while the blue contours represent the NFW fit.

Table 2
Results of the MCMC Parameter Estimation for the NFW Models and the NMC DM Model

Cluster	$c_{500,\rm GR}$	$M_{500,\rm GR}$ ($10^{14}\ M_\odot$)	$c_{500,\rm NMC}$	$M_{500,\rm NMC}$ ($10^{14}\ M_\odot$)	$L_{\rm NMC}$ (kpc)
A85	$2.0^{+0.1}_{-0.1}$	$6.2^{+0.2}_{-0.3}$	2.0 ± 0.2	$6.2^{+0.3}_{-0.3}$	12^{+6}_{-10}
A644	5^{+1}_{-2}	4.6 ± 0.4	$6.2^{+1.0}_{-1.7}$	4.6 ± 0.4	26^{+11}_{-4}
A1644	$1.1^{+0.2}_{-0.4}$	$3.2^{+0.3}_{-0.4}$	$1.4^{+0.3}_{-0.5}$	$3.3^{+0.3}_{-0.3}$	27^{+9}_{-3}
A1759	3.0 ± 0.2	$4.7^{+0.2}_{-0.3}$	$3.4^{+0.3}_{-0.3}$	$4.6^{+0.2}_{-0.2}$	20^{+7}_{-3}
A2029	$3.3^{+0.2}_{-0.3}$	7.7 ± 0.4	$3.6^{+0.3}_{-0.5}$	7.5 ± 0.4	28^{+15}_{-7}
A2142	$2.3^{+0.2}_{-0.2}$	8.4 ± 0.4	$2.4^{+0.2}_{-0.3}$	$8.4^{+0.4}_{-0.4}$	17.3^{+7}_{-15}
A2255	$1.6^{+0.4}_{-0.9}$	4.7 ± 0.4	$2.3^{+0.3}_{-0.7}$	4.8 ± 0.3	109^{+11}_{-8}
A2319	$3.8^{+0.4}_{-0.6}$	7.4 ± 0.2	$4.6^{+0.6}_{-0.8}$	7.4 ± 0.2	60^{+17}_{-5}
A3158	$2.0^{+0.3}_{-0.4}$	$4.0^{+0.3}_{-0.3}$	$2.6^{+0.4}_{-0.4}$	4.0 ± 0.2	36^{+6}_{-3}
A3266	$1.7^{+0.2}_{-0.2}$	6.6 ± 0.2	1.7 ± 0.2	$6.5^{+0.3}_{-0.3}$	15^{+5}_{-13}
RXC1825	$2.6^{+0.4}_{-0.4}$	$4.1^{+0.3}_{-0.3}$	$4.0^{+0.5}_{-0.9}$	3.5 ± 0.3	9^{+3}_{-8}
ZW1215	$1.5^{+0.2}_{-0.3}$	7.1 ± 0.7	$1.6^{+0.2}_{-0.3}$	7.0 ± 0.6	22^{+9}_{-19}

Note. The full set of parameter values and the related contours are available in the figure set.

responsible for the production of a hole-like feature (corresponding to low or negative values of pressure) observed in our analysis for a certain fraction of the cluster pressure profiles at inner radii. We, however, anticipate that these features could be erased just by adding one or more data points at inner radii for the pressure profiles. Unfortunately, such data are yet to be available for the X-COP cluster sample. In light of this, the reader should interpret values of the NMC length scale $L_{\rm NMC}$ obtained in this work for clusters exhibiting a hole in their pressure profiles just as upper bounds on the real values of $L_{\rm NMC}$. We also note that our NMC DM model does not modify the estimation of pressure profiles in the outskirts of the cluster, essentially implying that the results presented here are not degenerate with any additional physics that can potentially affect the pressure profile estimation at outer radii, such as nonthermal pressure support, which, for example, could be important for cluster A2319 (Eckert et al. 2019). In the last column of Table 1 we show estimates of the Bayesian evidence $\Delta_{\mathcal{B}}$ exploited to further compare the two models, assuming standard NFW to be the base model. The NMC DM model is preferred for half of the clusters in the sample, and likewise it is mildly disfavored by the other half (up to the more striking case of RXC1825, for which $\Delta_{\mathcal{B}} = -3.53$).

In Table 2 we have reported the concentration c and virial mass M_{500} values from our MCMC analysis for the NFW and the NMC DM models. Estimates for these values from the two models are always compatible within the displayed uncertainties, with the exception of cluster RXC1825's concentration (slightly larger in the NMC framework than the NFW case) and M_{500} (conversely slightly smaller in the NMC case). Despite this overall compatibility, we note that the NMC model predicts concentration values systematically larger than the NFW ones. Table 2 also features the MCMC estimations for the NMC length scale $L_{\rm NMC}$. Overall, these values of $L_{\rm NMC}$ exceed by 2 orders of magnitude, on average the same values obtained for spiral galaxies in Gandolfi et al. (2022). This result is remarkably consistent with the increasing trend observed for spiral galaxies in Gandolfi et al. (2022) between the mass of DM halos and the $L_{\rm NMC}$ associated with them, as we will show more in detail in Section 3.2.

In Figures 1 and 2 we show two exemplificative profiles (clusters A644 and A2142) obtained with our MCMC analysis, alongside the posterior contour plots for the $\{M_{500}, c, L_{\rm NMC}\}$. As in the other clusters, both the NFW and the NMC DM models provide a good description of the general trend of the data. However, the NMC DM model is able to provide a better fit for the clusters whose data at the innermost radii are tracing a flattening in the shape of the pressure profiles. Such flattening seems to arise right within the area in which the NMC effect is active (i.e., within a distance of $L_{\rm NMC}$ from the center of the

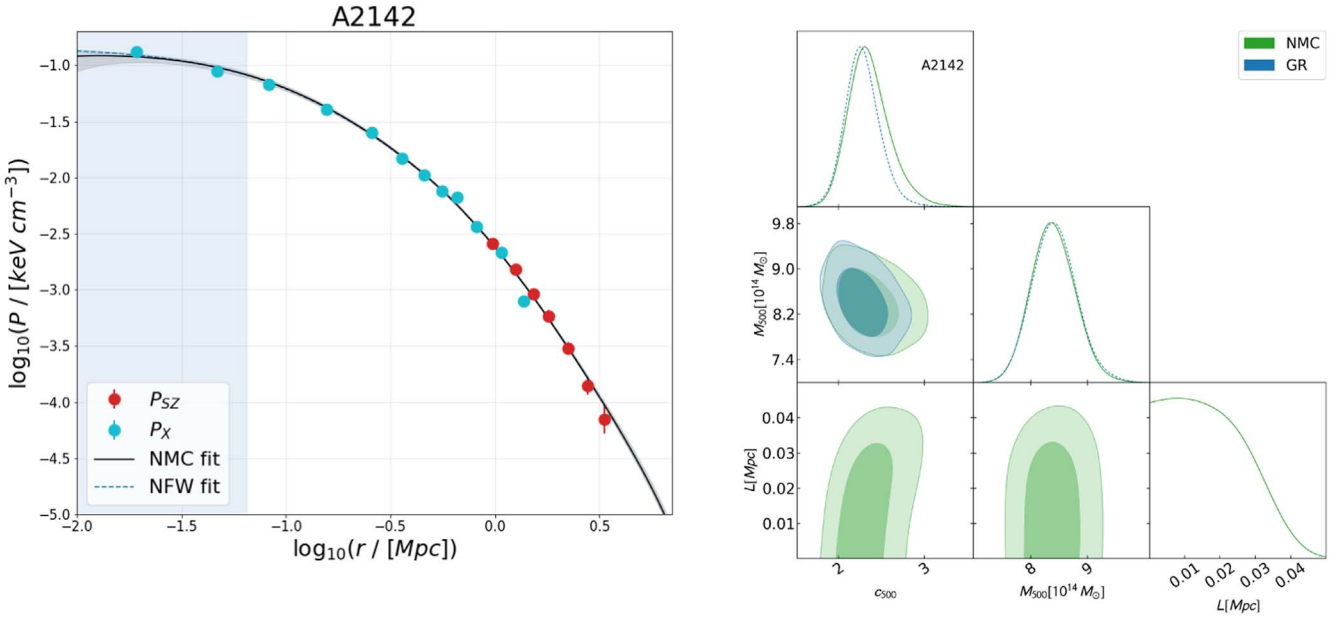

Figure 2. Same as Figure 1 but for the A2142 cluster.

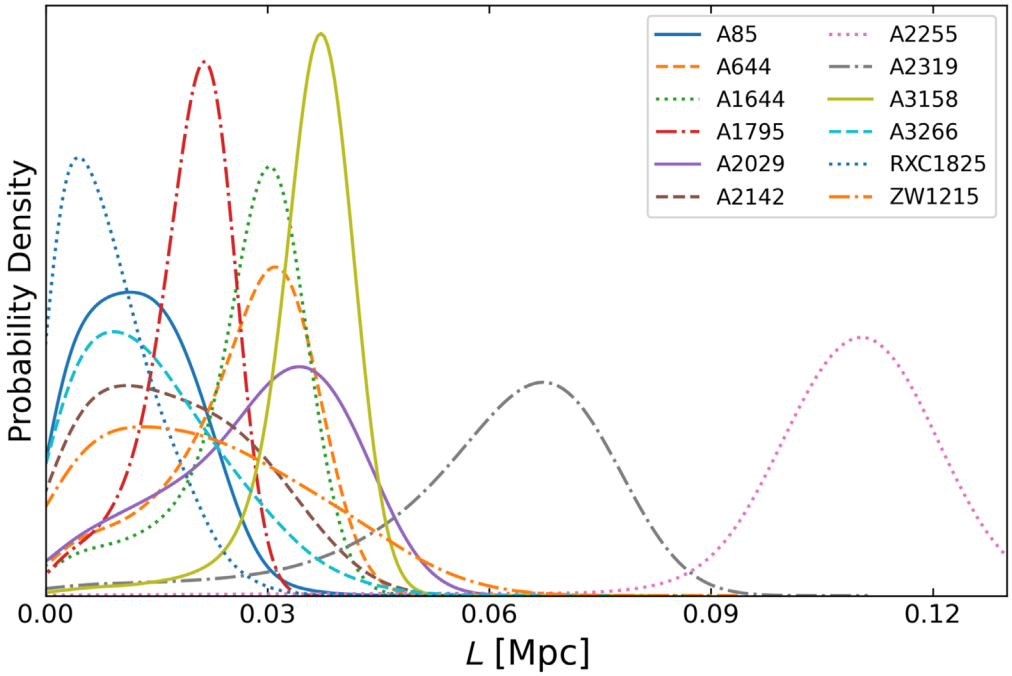

Figure 3. The one-dimensional posterior distribution for the length scale parameter $L_{\rm NMC}$ as retrieved in our Bayesian MCMC analysis.

dark haloes, represented as a blue shaded area in both Figures 1 and 2). As mentioned before, such an NMC effect should be read with caution, given the limitation of the temperature data available in the innermost regions of the cluster.

Figure 3 shows the one-dimensional posterior distribution of the $L_{\rm NMC}$ parameter from our MCMC analysis for the X-COP cluster sample. Consistently with the galactic dark halos analyzed in Gandolfi et al. (2022), $L_{\rm NMC}$ has different values in different halos, depending on their characteristics (in particular on their virial mass). Some halos (e.g., RXC1825 or A85) show a one-dimensional posterior converging toward $L_{\rm NMC} = 0$, suggesting that the DM density profile for these halos may have a cuspy shape, well reproduced by the NFW model. In other halos (e.g., A2319 and A2255) the NMC produces typical scale lengths capable of reaching fractions of megaparsecs. These values are likely to be slightly overestimated since, as previously discussed, some of these clusters exhibit an NMC DM pressure profile featuring a central hole. Despite this, the peak of such a one-dimensional posterior is clearly far from $L_{\rm NMC} = 0$, indicating that the shape of the density profile of these dark halos could be less cuspy and different from that of the NFW profile. As can be seen in the right panel of Figure 1, the nonzero values for $L_{\rm NMC}$ are essentially accompanied by a mild positive correlation with M_{500} and subsequently a non-Gaussian degeneracy with the concentration c. Also, for all the clusters that have a nonzero posterior for the $L_{\rm NMC}$, we do not observe any such correlation with the M_{500}

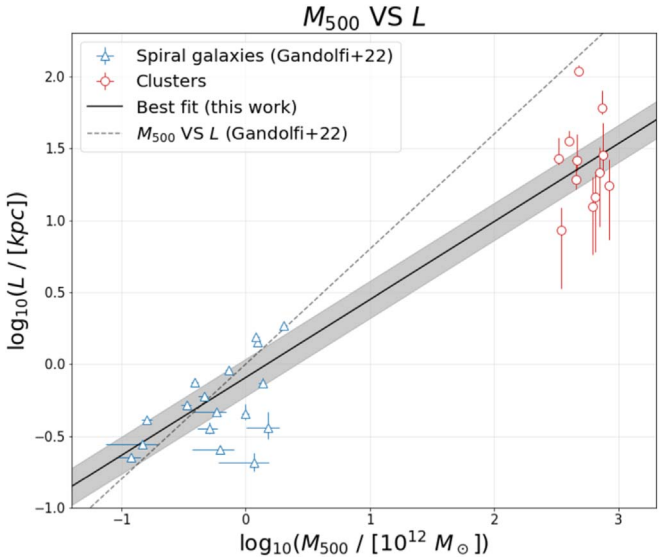

Figure 4. Virial mass (M_{500}) vs. $L_{\rm NMC}$ relation. Blue triangles are the same spiral galaxies' data utilized in Gandolfi et al. (2022), whereas the red circles represent the X-COP cluster measurements found in our Bayesian MCMC analysis. The best-fit power law is represented as a solid black line, whereas the shaded gray area represents a 1σ confidence interval. The gray dashed line represents the M_{500} vs. $L_{\rm NMC}$ relation utilized in Gandolfi et al. (2022) to obtain the results therein. Note that the virial masses of spirals and their errors are rescaled to M_{500} (i.e., a mass at which the interior mean density is 500 times the critical density of the universe) since they were originally computed as M_{200} (i.e., a mass at which the interior mean density is 200 times the critical density of the universe).

parameter, as in the case of A2142, shown in the right panel of Figure 2. In this context, clusters A2255 and A2319 show a slightly larger value of the length scale $L_{\rm NMC}$ in the posteriors. We also note that for the clusters A2255 and RXC1825, we find a strong bimodal behavior, from which we select the maximum posterior region. As can be seen also from the corresponding Bayesian evidence in favor of the NMC DM model, the clusters A3158, A2319, and A2255 show a moderate preference ($\Delta_{\log(\mathcal{B})} \gtrsim 2$), owing to the slightly larger values of $L_{\rm NMC}$. As can be seen in Figure 6 in the Appendix, this evidence in favor of the NMC DM in these three clusters is essentially driven by the improvement of the fit accounting for the innermost data point in the X-ray pressure observations. And on the contrary, the cluster RXC1825 shows a preference for the standard NFW scenario at a similar level of Bayesian evidence.

3.2. L_{NMC} *versus* M_{500}

In this section, we investigate the relation between the NMC length scale $L_{\rm NMC}$ and the dark halo virial mass M_{500} observed as a result of our analysis. We remark that this relationship is an important feature of the NMC DM model which, as previously stated, is not to be considered as a modified theory of gravity, and therefore $L_{\rm NMC}$ should not be thought of as a new proposed fundamental constant of nature. The observed relationship between $L_{\rm NMC}$ and M_{500} shows that $L_{\rm NMC}$ indeed does not have a universal value, and it depends on at least one property of the dark haloes under consideration. The $L_{\rm NMC}$–M_{500} relationship was first observed in Gandolfi et al. (2022) to hold for the galactic dark halos, analyzed therein. A remarkable result of this earlier analysis is that one can describe such a relationship with a simple power law. In this work, we investigate the validity of this relation up to the virial mass ranges typical of galaxy clusters. The results of our analysis are shown in Figure 4. Here, the virial masses of the spiral galaxies and their errors are rescaled from M_{200} to M_{500} to homogenize the results. Remarkably, the X-COP clusters data point derived by our MCMC analysis are seemingly in agreement with the power-law trend of the $L_{\rm NMC}$–M_{500} relationship observed in Gandolfi et al. (2022). We performed an MCMC fit using the model $\log_{10} L_{\rm NMC} = a \log_{10}(bM_{500})$ to fit both galactic and clusters data simultaneously, obtaining as parameter values $a = 0.542 \pm 0.005$ and $b = 0.807 \pm 0.005$. The slope a found in this analysis is compatible with the slope found by fitting a similar power law to galaxies only, as done in Gandolfi et al. (2022; 0.7 ± 0.2). The best-fit line in this work is shown in Figure 4 as a solid black line together with a gray shaded area representing a 1σ confidence limit of the fit. In the same figure, we also show as a gray dotted line the relation $L_{\rm NMC} = M_{200}^{0.8}$, utilized in Gandolfi et al. (2022) as a reference relation to study the capacity of the NMC DM model in reproducing the radial acceleration relation (RAR). In the galactic virial mass regime, the two power laws are consistent within a 1σ confidence limit, and their slopes are compatible within the errors. The updated scaling law retrieved in this work translates into an average variation of the RAR with respect to the one computed in Gandolfi et al. (2022) by a mere 0.33%, with the average of such variation being taken for every radial acceleration bin in which the RAR of Gandolfi et al. (2022) is computed (spanning from a minimum variation of 0.004%–1.4% among all the bins). We stress that such variation is well within the errors associated to the RAR computed in Gandolfi et al. (2022) for every single bin of radial acceleration. In fact, for the RAR of Gandolfi et al. (2022) the minimum and maximum percentage relative uncertainties are 0.67% and 3.27%, respectively, and the average one is 1.85%. We thus conclude that the updated $L_{\rm NMC}$–M_{500} relation retrieved in this work, albeit different from the one considered in Gandolfi et al. (2022), is still able to reproduce the RAR in the galactic dark haloes mass regime. That being said, from Figure 4 it is possible to appreciate the significant difference between the two power laws when approaching the cluster dark halo mass regime. This essentially constitutes an improvement over the previous analysis, which utilized only the galaxies to assess the same relation. As previously mentioned, for some of the clusters, the $L_{\rm NMC}$ values could be slightly overestimated, and hence it is possible that the real best-fit power law could be even less steep than what is found in our analysis. Moreover, we expect that including a galaxy cluster dataset that probes the innermost regions of the halo could help reduce the scatter in the $L_{\rm NMC}$–M_{500} relation.

3.3. *Scatter in the* M_{500} *versus* c

In Figure 5 we test the correlation between concentration c and M_{500} values inferred from our MCMC analysis against the relationship between c_{200} and M_{200} of dark halos found in Dutton & Macciò (2014), namely:

$$\log_{10} c_{200} = 0.905 - 0.101 \log_{10}(M_{200}/10^{12} h^{-1}\, M_\odot). \quad (8)$$

To make this comparison, we rescale the value of the virial mass M_{500} of the clusters to M_{200}, recalculating the corresponding concentrations accordingly. We then perform an MCMC fit to find the best-fit power law that best describes the data obtained by exploiting both the NFW model and the NMC DM model. In both these cases, there is some visible

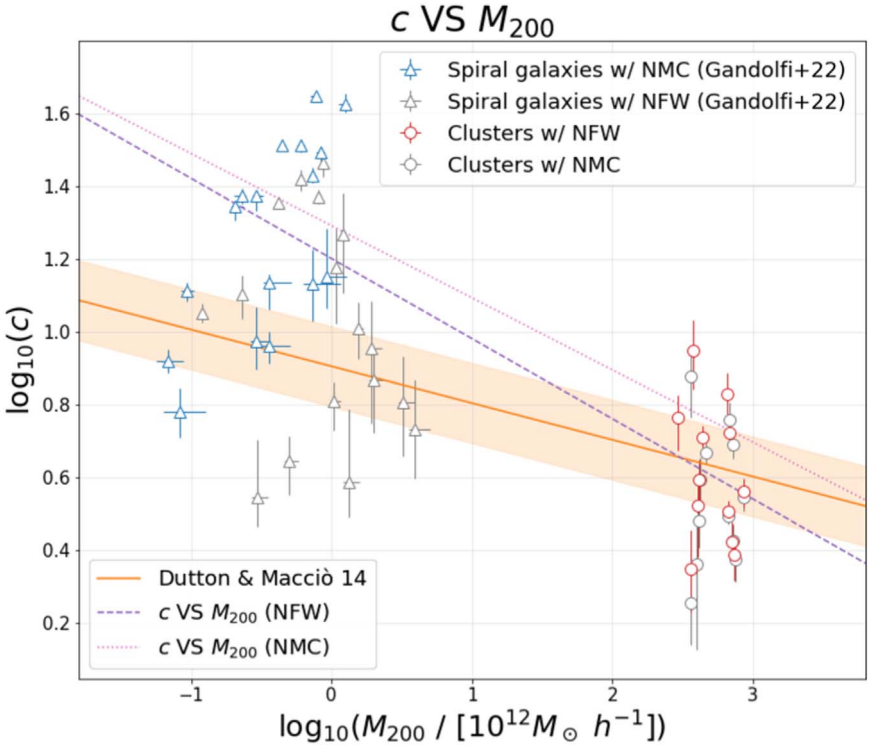

Figure 5. Concentration vs. virial mass relation. Gray triangles and gray circles are, respectively, spiral galaxies from Gandolfi et al. (2022) and X-COP clusters' data obtained with the NFW model. Blue triangles and red circles represent data retrieved assuming the NMC DM model. The orange solid line represents the relation by Dutton & Macciò (2014) featuring a lognormal scatter of 0.11 dex represented by the orange area around the line. The purple dashed line and the pink dotted lines represent, respectively, the c_{200} vs. M_{200} relations, respectively, found for the NFW model and the NMC DM model. Note that the cluster virial masses (M_{500}) and their errors have been downscaled to M_{200} to make them comparable to the Dutton & Macciò (2014) relation.

difference between the two best-fit power laws and the relationship found in Dutton & Macciò (2014). This is true at least up to the cluster mass regime, where both the best-fit power laws of the NFW and NMC DM model intersect the report of Dutton & Macciò (2014). Comparing the best-fit power laws with each other, we do not identify important differences between the two models since the corresponding data have a rather similar scatter around the Dutton & Macciò (2014) relation. This is something we expected following the previous examination of the tabulated results of our MCMC analysis. Figure 5 can provide interesting qualitative hints on the expected concentrations of sub-haloes in galaxy clusters within this framework. As shown in Meneghetti et al. (2020), the ΛCDM is at variance with the observed density and compactness of the DM sub-haloes in galaxy clusters. From our analysis, the NMC DM model predicts galaxy-sized DM substructures in clusters featuring overall higher concentrations associated with lower halo mass values with respect to the standard CDM paradigm. However, we give the caveat that only future analysis relying on high-quality data and exploiting a larger sample of galaxy clusters can confirm this prediction. In this context, the observed tensions at galaxy clusters scales present a promising way to further test the NMC DM scenario and its phenomenology.

4. Summary

In this section, we summarize the main results of this work. We tested the NMC DM model against the pressure profiles of galaxy clusters belonging to the X-COP sample, finding that:

1. Our model in which the NMC acts as a perturbation over a cold DM behavior provides a good description of the cluster pressure profiles, with a fit accuracy comparable to or in some cases even better than the NFW model both in terms of reduced χ^2 and Bayesian evidence.
2. The M_{500}–$L_{\rm NMC}$ relation is well described by a simple power law even beyond the mass regime of spiral galaxies investigated in Gandolfi et al. (2022). However, to extend this relationship to include galaxy clusters, it is necessary to correct the slope of the above relationship with respect to the value reported in Gandolfi et al. (2022) based only on late-type galaxies.

One key issue in our analysis is the lack of data at smaller radii in the pressure profiles of the X-COP clusters, as this may have partially resulted in overestimating the $L_{\rm NMC}$ values inferred in our analysis. Nevertheless, previous works based on X-COP cluster data (see, e.g., Haridasu et al. 2021) highlighted how cored profiles would seem to better describe the DM density distribution for a few clusters belonging to this sample. Then, even if the X-COP cluster profiles were better characterized at inner radii, the NMC DM model would probably be still preferred for all those clusters exhibiting cored profiles with respect to the cuspier NFW model. Indeed, a possible future step to corroborate our analysis would be to use data from well-characterized galaxy clusters at small radii (such as data from the CLASH collaboration; see, e.g., Umetsu et al. 2014), probing the regions where the effect of the NMC is crucial. Another interesting extension of our work would concern the investigation of the mechanism originating the NMC between DM and gravity and particularly how this mechanism gives rise to the observed power-law relationship

between $L_{\rm NMC}$ and the virial mass M_{500}. For this purpose, we will consider implementing the NMC DM model in full N-body simulation to study the time-dependent conditions and the formation mechanisms of cosmic structures in this framework. In this context, colliding galaxy clusters would configure as promising study systems to place constraints on the NMC DM model, in a similar fashion to what is done with self-interacting DM scenarios (see, e.g., Robertson et al. 2017). Indeed, the effects of the NMC in colliding systems could be particularly significant in the regions where the DM density changes appreciably as a consequence of the DM haloes merger. Indeed, we expect the repulsive nature of the NMC to manifest at the interface of the collision, with the overall effect of slowing down the merger process. Modeling this scenario is, however, challenging and calls for dedicated future work. We also stress that another interesting avenue to characterize the phenomenology of this model further is to test it against known tensions on galaxy cluster scales and beyond.

Acknowledgments

We warmly thank Dominique Eckert for sharing additional data with us, and we thank the anonymous referee for the helpful and constructive comments. A.L. is supported by the EU H2020-MSCA-ITN-2019 Project 860744 BiD4BESt: Big Data applications for black hole Evolution Studies, and by the PRIN MIUR 2017 prot. 20173ML3WW: Opening the ALMA window on the cosmic evolution of gas, stars and supermassive black holes. B.S.H. is supported by the INFN INDARK grant.

Appendix
Pressure Profiles

In Figure 6, we show the pressure profiles reconstructed for the NMC DM case for each of the 12 clusters.

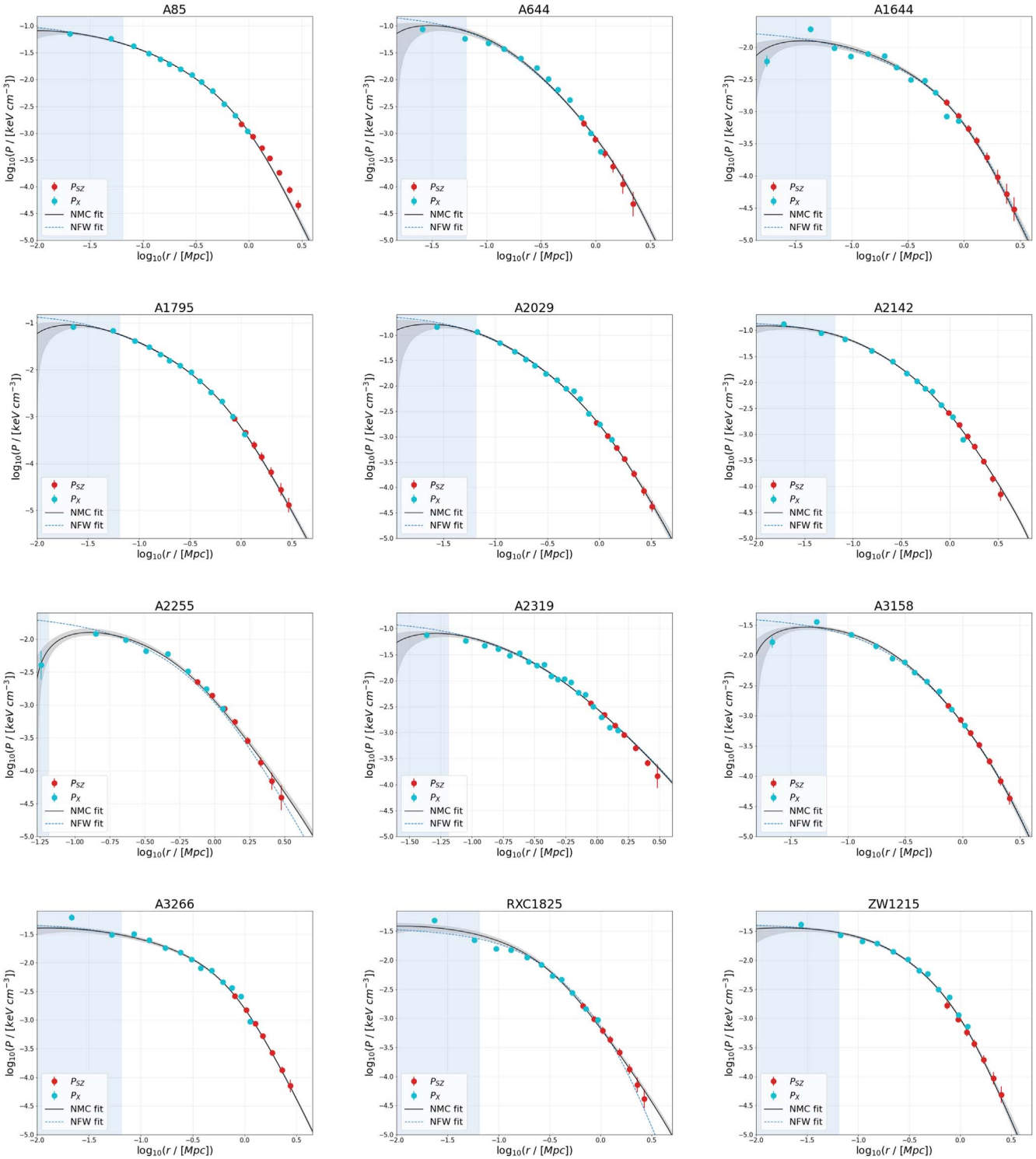

Figure 6. We show the comparison of the pressure profiles for the NMC DM model (solid lines) against those of the NFW model (dashed gray lines) for all the 12 clusters in X-COP compilation.

ORCID iDs

Giovanni Gandolfi https://orcid.org/0000-0003-3248-5666
Balakrishna S. Haridasu https://orcid.org/0000-0002-9153-1258
Stefano Liberati https://orcid.org/0000-0002-7632-7443
Andrea Lapi https://orcid.org/0000-0002-4882-1735

References

Aghanim, N., Akrami, Y., Ashdown, M., et al. 2020, A&A, 641, A6
Behroozi, P. S., Wechsler, R. H., & Conroy, C. 2013, ApJ, 770, 57
Bekenstein, J. D. 1993, PhRvD, 48, 3641
Bertolami, O., & Paramos, J. 2010, JCAP, 2010, 009
Bettoni, D., Colombo, M., & Liberati, S. 2014, JCAP, 2014, 004
Bettoni, D., & Liberati, S. 2015, JCAP, 2015, 023

Bettoni, D., Liberati, S., & Sindoni, L. 2011, JCAP, 2011, 007
Bettoni, D., Pettorino, V., Liberati, S., & Baccigalupi, C. 2012, JCAP, 2012, 027
Bosma, A. 1978, PhD thesis, Univ. Groningen
Boylan-Kolchin, M., & Ma, C.-P. 2004, MNRAS, 349, 1117
Bruneton, J.-P., Liberati, S., Sindoni, L., & Famaey, B. 2009, JCAP, 2009, 021
Burkert, A. 1995, ApJL, 447, L25
Burkert, A. 2015, ApJ, 808, 158
Burkert, A. 2020, ApJ, 904, 161
Chae, K.-H., Bernardi, M., Sheth, R. K., & Gong, I.-T. 2019, ApJ, 877, 18
de Blok, W. J. G. 2010, AdAst, 2010 789293
Desmond, H. 2017, MNRAS, 464, 4160
Di Casola, E., Liberati, S., & Sonego, S. 2015, AmJPh, 83, 39
Di Cintio, A., Brook, C. B., Dutton, A. A., et al. 2014, MNRAS, 441, 2986
Di Cintio, A., & Lelli, F. 2016, MNRAS, 456, L127
Di Paolo, C., Salucci, P., & Fontaine, J. P. 2019, ApJ, 873, 106
Donato, F., Gentile, G., Salucci, P., et al. 2009, MNRAS, 397, 1169
Dutton, A. A., & Macciò, A. V. 2014, MNRAS, 441, 3359
Eckert, D., Ettori, S., Pointecouteau, E., et al. 2017, AN, 338, 293
Eckert, D., Ghirardini, V., Ettori, S., et al. 2019, A&A, 621, A40
El-Zant, A., Freundlich, J., & Combes, F. 2016, MNRAS, 461, 1745
Ettori, S., Ghirardini, V., Eckert, D., et al. 2019, A&A, 621, A39
Foreman-Mackey, D., Hogg, D. W., Lang, D., & Goodman, J. 2013, PASP, 125, 306
Freundlich, J., Dekel, A., Jiang, F., et al. 2020a, MNRAS, 491, 4523
Freundlich, J., Jiang, F., Dekel, A., et al. 2020b, MNRAS, 499, 2912
Gandolfi, G., Lapi, A., & Liberati, S. 2021, ApJ, 910, 76
Gandolfi, G., Lapi, A., & Liberati, S. 2022, ApJ, 929, 48
Ghirardini, V., Eckert, D., Ettori, S., et al. 2019, A&A, 621, A41
Ghirardini, V., Ettori, S., Eckert, D., et al. 2018, A&A, 614, A7
Green, M. A., & Moffat, J. W. 2019, PDU, 25, 100323
Haridasu, B. S., Karmakar, P., De Petris, M., Cardone, V. F., & Maoli, R. 2023, PhRvD, 107, 124059
Heavens, A., Fantaye, Y., Mootoovaloo, A., et al. 2017a, arXiv:1704.03472
Heavens, A., Fantaye, Y., Sellentin, E., et al. 2017b, PhRvL, 119, 101301
Hogg, D. W., & Foreman-Mackey, D. 2018, ApJS, 236, 11
Ivanov, D., & Liberati, S. 2020, JCAP, 2020, 065
Jeffreys, H. 1961, The Theory of Probability (Oxford: Oxford Univ. Press)
Keller, B. W., & Wadsley, J. W. 2017, ApJL, 835, L17
Lelli, F., McGaugh, S. S., Schombert, J. M., & Pawlowski, M. S. 2017, ApJ, 836, 152
Lewis, A. 2019, arXiv:1910.13970
Li, P., Lelli, F., McGaugh, S., & Schombert, J. 2018, A&A, 615, A3
Łokas, E. L., & Mamon, G. A. 2001, MNRAS, 321, 155
Ludlow, A. D., Benítez-Llambay, A., Schaller, M., et al. 2017, PhRvL, 118, 161103
Meneghetti, M., Davoli, G., Bergamini, P., et al. 2020, Sci, 369, 1347
Milgrom, M. 1983, ApJ, 270, 365
Navarro, J. 2006, in KITP Conf.: Applications of Gravitational Lensing: Unique Insights into Galaxy Formation and Evolution, 30, ed. L. V. E. Koopmans et al. (Santa Barbara, CA: KITP)
Navarro, J. F., Benítez-Llambay, A., Fattahi, A., et al. 2017, MNRAS, 471, 1841
Navarro, J. F., Frenk, C. S., & White, S. D. M. 1996, ApJ, 462, 563
Peirani, S., Dubois, Y., Volonteri, M., et al. 2017, MNRAS, 472, 2153
Planck Collaboration, Ade, P. A. R., Aghanim, N., et al. 2016, A&A, 594, A24
Pontzen, A., & Governato, F. 2014, Natur, 506, 171
Robertson, A., Massey, R., & Eke, V. 2017, MNRAS, 465, 569
Rodrigues, D. C., & Marra, V. 2020, in IAU Symp. 359, Galaxy Evolution and Feedback across Different Environments (Cambridge: Cambridge Univ. Press), 457
Rubin, V. C., Ford, W. K. J., & Thonnard, N. 1978, ApJL, 225, L107
Salucci, P. 2019, A&ARv, 27, 2
Salucci, P., & Burkert, A. 2000, ApJL, 537, L9
Santos-Santos, I. M., Brook, C. B., Stinson, G., et al. 2016, MNRAS, 455, 476
Tian, Y., Umetsu, K., Ko, C.-M., Donahue, M., & Chiu, I.-N. 2020, ApJ, 896, 70
Trotta, R. 2008, ConPh, 49, 71
Trotta, R. 2017, arXiv:1701.01467
Umetsu, K., Medezinski, E., Nonino, M., et al. 2014, ApJ, 795, 163
Vikhlinin, A., Kravtsov, A., Forman, W., et al. 2006, ApJ, 640, 691
Wheeler, C., Hopkins, P. F., & Doré, O. 2019, ApJ, 882, 46
Zwicky, F. 1933, AcHPh, 6, 110